Article

Molecular Doping for Hole Transporting Materials in Hybrid Perovskite Solar Cells

Vanira Trifiletti [1,2,3,*], Thibault Degousée [1], Norberto Manfredi [2], Oliver Fenwick [1], Silvia Colella [3,4], and Aurora Rizzo [4]

[1] School of Engineering and Materials Science (SEMS), Queen Mary University of London, Mile End Road, London E1 4NS, UK.

[2] Department of Materials Science and Milan - Bicocca Solar Energy Research Center – MIB-Solar University of Milan - Bicocca, Via Cozzi 55, 20125, Milano, Italy.

[3] Department of Mathematics and Physics "E. De Giorgi" University of Salento, Lecce, 73100, Italy

[4] Istituto di Nanotecnologia CNR-Nanotec, Polo di Nanotecnologia c/o Campus Ecotekne via Monteroni, 73100 Lecce, Italy.

* Correspondence: v.trifiletti@qmul.ac.uk; Tel.: +44 (0)20 7882 5306

Abstract: Hybrid lead halide perovskites have been revolutionary in the photovoltaic research field, reaching efficiencies comparable with the most established photovoltaic technologies, although they do not yet reach their competitor stability. The search for a stable configuration required the engineering of the charge extraction layers; in this work, molecular doping is used as an efficient method for small molecule and polymer, employed as hole transport materials in planar heterojunction configuration on compact-TiO_2. We proved the viability of this approach, obtaining significantly increased performances and reduced hysteresis on compact titania-based devices. We investigated the photovoltaic performance, correlating to the hole transport material structure. We have demonstrated that the molecular doping mechanism is more reliable than the oxidative doping and verified that molecular doping in polymeric hole transport materials leads to highly efficient perovskite solar cell, with long-term stability.

Keywords: molecular doping; perovskite solar cell; stability; hysteresis; F4-TCNQ

1. Introduction

Hybrid lead halide perovskites are revolutionary materials for a wide range of optoelectronic and electronic applications [1-3]. In the photovoltaic research field, they have shown efficiencies comparable with the most established photovoltaic technologies, overcoming the thin-film technologies, although perovskite-based solar cells do not yet reach their competitor's stability [1,4-6]. A step forward to achieve devices with long-term stability has recently been achieved with mixed-cation lead mixed-halide perovskites, such as $(HC(NH_2)_2))_{0.83}Cs_{0.17}Pb(I_{0.6}Br_{0.4})_3$ [7,8]. Therefore, the search for the most stable configuration is, nowadays, dominated by the search for charge extractor materials that can stabilise the solar cell performance [4,9]. In a conventional device architecture (substrate; cathode; Electron Transporting Material, ETM; hybrid perovskite; Hole Transporting Material, HTM; anode), the most commonly HTM employed, thanks to the significant solubility and excellent hole mobility, is Spiro-OMeTAD (2,2′,7,7′-Tetrakis N, N-di-p-methoxyphenylamine)-9,9′-spirobifluorene) [10,11]. Spiro-OMeTAD has given excellent results: the doping occurs by oxidation of the complex that it forms with the additive LiTFSI (bis(trifluoromethylsulphonyl)imide) in open system condition. However, it is hard to collect consistent results because the amount of oxidised Spiro-OMeTAD depends on external factors (oxygen in the active layer, light intensity, humidity, room temperature). The fluctuation of the oxidised Spiro-OMeTAD concentration affects device stability and reproducibility [12], and the Li+ cations can easily migrate across the perovskite film and reach the ETL interface, with massive impact on the hysteresis [13].

In order to address this issue, other organic materials have been successfully employed as HTMs in perovskite solar cells, such as P3HT, poly(3-hexylthiophene-2,5-diyl) [14], that has a higher hole mobility (up to 0.1 cm^2 V^{-1} s^{-1} in LiTFSI-doped P3HT compared to 10^{-4} cm^2 V^{-1} s^{-1} in LiTFSI-doped Spiro-OMeTAD) [15]. Lately, polymeric HTMs are attracting attention because the film structure is not affected by the working operation condition, and they can form an adequate barrier to prevent gold migration from the back contact [16]. With the aim of decrease the production costs, the interest in the study of P3HT as HTM in perovskite solar cell is much increased: it is a well-known material, and it is easy to coat [14,17-20]. Undoped P3HT has proven to be extremely effective: tested on perovskite films with very low defect densities and engineered interface, it achieved high solar conversion efficiencies [14,21]. Still, long-term stability remains an issue. The most remarkable result to date is, after 1,008 h under 85% relative humidity at room temperature, retention of 80% of the initial efficiency [14]. A way to increase stability is to exploit the molecular doping methodology. Doping technology is extensively used in photovoltaic and electroluminescent devices, based on inorganic, organic and hybrid materials, to enhance the conductivity of the transporting layers [22]. Besides, doping has proven to be an effective way to increase stability in organic photovoltaic devices, and a large variety of molecular species can serve as dopants in organic semiconductors [23-25].

In this study, F4-TCNQ (2,3,5,6-Tetrafluoro-7,7,8,8-tetracyanoquinodimethane) has been employed [26-29] as an additive in a small molecule HTM (Spiro-OMeTAD) and polymer HTM (P3HT). F4-TCNQ is a strong electron acceptor and widely used as hole selective layer or as an additive in p-type doping [26,30-36]. F4-TCNQ is commonly used to minimise the hole injection barrier: it has been proven that F4-TCNQ doping generates a polaron charge-transfer complex that increases the HTM conductivity and decreases the charge recombination [37]. Huang et al. [38] reported about F4-TCNQ:Spiro-OMeTAD as HTM layer to improve air stability of perovskite solar cells. Their device reaches 10.6% efficiency (PCE), comparable to LiTFSI doping (PCE = 12.7%). However, the F4-TCNQ-based devise retains 85% of this PCE after 72 hours and 60% after 1 week of the first performance, compared with the LiTFSI-based device that retains 20% after 72 hours and 10% after 1 week of the initial performance. They attributed the increased stability to the substitution of hygroscopic Li-TFSI with the non-hygroscopic F4-TCNQ. Encouraged by the results mentioned above, we tested F4-TCNQ doping, in various concentration, in the planar heterojunction configuration on compact-TiO_2 (c-TiO_2:PHJ, **Figure 1** in relief): in this device architecture, the ETM is only composed by a layer of about 80 nm of titania, and no scaffold is used. [39] In order to obtain reliable $CH_3NH_3PbI_3$ layers, they have been grown following the procedure published by us elsewhere [40]. As demonstrated by the high efficiencies that the fine engineering of the absorber layer and its interface with the charge extraction layers can provide [14,41,42], we employed a compact perovskite film with reduced surface defects and large grain size, in order to realise devices with photovoltaic performance independent on the voltage scan direction. Scanning electron microscopy (SEM) image of the employed perovskite film is shown in **Figure 1b**.

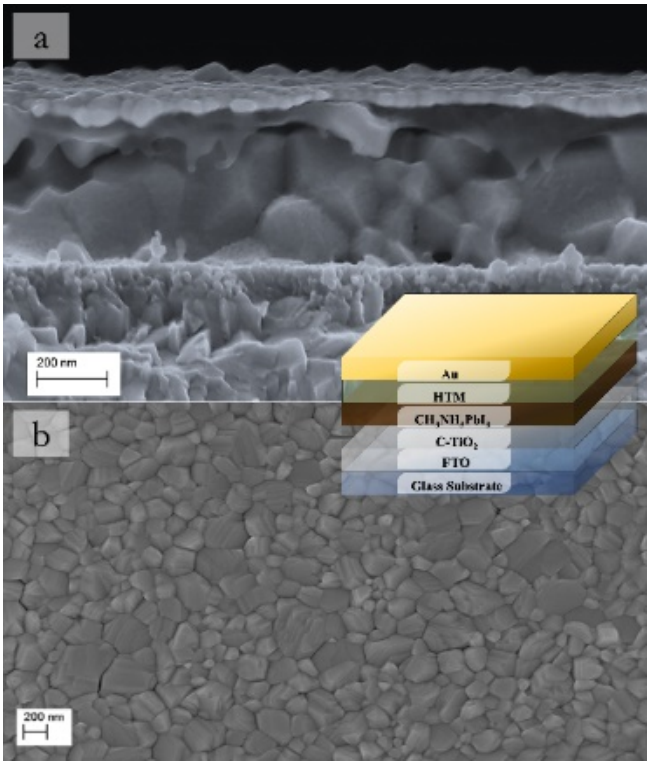

Figure 1. Scanning electron microscopy (SEM) images of: a) the device cross-section, and b) employed $CH_3NH_3PbI_3$ perovskite film; cartoon of the device structures in relief.

2. Materials and Methods

Hybrid perovskite solar cells were prepared in a planar heterojunction configuration on compact-TiO_2 (c-TiO_2:PHJ) (relief in **Fig. 1**); LiTFSI doped Spiro-OMeTAD was employed as a control device [40]. Fluorine tin oxide (FTO)/glass was employed for the substrate and was partially etched. Substrate cleaning was performed using pure water, acetone, and isopropanol in an ultrasonic bath. Then, they were immersed in a TL1 washing solution, that was heated up to 80 °C (10 min), then they were rinsed by using pure water. The TiO_2 was synthesised by twice spin coating 0.15 M of titanium diisopropoxidebis(acetylacetonate) solution in 1-butanol, and once spin coating 0.3 M of titanium diisopropoxidebis(acetylacetonate) solution in 1-butanol. After each deposition, the sample was heated on a hot plate at 125 °C for 5 min, and then heated for 2 h in an oven at 520 °C [40].

CH_3NH_3I was synthesised according to the procedure reported in the literature [45]. The 2 M $CH_3NH_3PbI_3$ solution has been prepared according to the procedure published by us elsewhere [40]: (i) the PbI_2 pellets were solved in a mixture of γ-butyrolactone, and dimethyl sulfoxide for 1 h at 90 °C and the CH_3NH_3I powder added; (ii) the mixture of PbI_2 pellets and CH_3NH_3I powder was stirred for 30 min at 70 °C and kept overnight at 60 °C. The day after, 200 μL was dropped and spin-coated on the TiO_2/FTO at 1000 and 4000 rpm, respectively for 20 and 60 s. During the final spin-coating step, 200 μL of dichloromethane were dropped. The samples were then annealed for 75 min at 100 °C on a hot-plate, subjected for four 4 h to 9.0×10^{-7} mBar [40].

The Spiro-OMeTAD in chlorobenzene concentration was 63 mg mL^{-1}, and it was doped by tert-butylpyridine (27.8 μL) and LiTFSI in acetonitrile solution (30.7 μL). The spin rate was 2500 rpm for 45 s, in order to produce a layer of 90 nm. Spiro-OMeTAD doped with F4-TCNQ (Sigma-Aldrich) were prepared in 0.1, 0.5, 1 and 5 wt%. The doped solutions were spun at a rate of 2500 rpm for 45 seconds. We, therefore, extended this approach to P3HT (Regioregularity ≥ 98%, Sigma-Aldrich), as proof of concept: we used a 15 mg mL^{-1} solution in chlorobenzene, stirred at 80 °C for 10 minutes. Once cooled down to room temperature, 100 μL of the filtered solution was spin-coated onto the perovskite film at 600 and 2000 RPM for, respectively, 12 and 40 seconds [17]. The coated films were then annealed on a hot-plate set at 100 °C for 10 minutes, to increase the order in the P3HT film

structure [43]. P3HT film thickness was about 60 nm. Various amounts of F4-TCNQ were added to the P3HT solution to change the doping concentration. The coating of the perovskites films was unchanged for both type HTM doped layers. Finally, 80 nm Au electrodes were grown by thermal evaporation.

MERLIN Zeiss SEM FEG instrument was employed for scanning electron microscopy, at an accelerating voltage of 5 kV. A monochromator (Omni 300 LOT ORIEL) with a single grating in Czerny-Turner optical design, in AC mode with a chopping frequency of 13 Hz and light bias (1 sun) applying was used for recording the external quantum efficiency. A Keithley 2400 Source Measure Unit and a solar simulator Spectra Physics Oriel 150 W, with AM1.5G filter set were used to measure the current-voltage characteristics. Devices were tested inside and outside the glovebox, without encapsulation. Devices were tested with a humidity of 50% under ambient conditions. The reported performances are registered after 30 minutes in air. Shunt (R_{sh}) and Series resistance (R_s) has been evaluated assuming the single diode model [44]: R_{sh} can be approximated by the negative of inverse slope of the characteristic curve where the voltage is null, and R_s can be approximated by the negative of inverse slope of the characteristic curve where the current is null.

3. Results and Discussion

In order to verify the reliability of each set of measurement, devices employing undoped and F4-TCNQ doped Spiro-OMeTAD were fabricated; LiTFSI doped Spiro-OMeTAD was also tested as a control device. F4-TCNQ 0.1 wt% doping is effective, compared with the undoped Spiro-OMeTAD. The significant increase in current of the F4-TCNQ doped films induces an almost two-fold increased efficiency, reaching similar PCE as the LiTFSI doping method. This result demonstrates the efficient F4-TCNQ doping effect, and notably, the 0.1wt% device does not present hysteresis (best devices in **Table 1**). The average PCE on 4 devices are 6.38 ± 0.45, 11.60 ± 0.15, 8.79 ± 0.30, 7.63 ± 0.24, 6.45 ± 0.30 for undoped, 0 wt%, 0.1 wt%, 0.5 wt%, 1 wt%, and 5 wt% F4-TCNQ doping respectively. Increasing the molecular doping to 0.5wt% a sharp drop in current is clear, which is accompanied by a drop-in potential over 1wt% doping. This decrease in performance was predictable, considering the tendency of F4-TCNQ to create aggregates in mixtures with other molecules [45]. It has been shown that beyond specific doping, the increase in photocurrent is accompanied by an increase in series resistance, caused by insulating aggregates [45-48]. Therefore, we can conclude that p-type molecular doping by careful tuning of the dopant weight per cent is promising to enhance photovoltaic performances of perovskites cells. Although, for Spiro-OMeTAD, the control LiTFSI-based device exhibits superior performance (Jsc = 19,67; Voc = 1.08; FF = 0.67; PCE = 14.23; HI = 0.00), as already reported previously [38].

Table 1. Photovoltaic performance of the best $CH_3NH_3PbI_3$ solar cells varying the p-type doping (where HI is Hysteresis Index, defined by Calado et al. [49]).

HTM	F4-TCNQ doping (wt%)	J_{sc} (mA cm^{-2})	V_{oc} (V)	FF	PCE (%)	HI
Spiro-OMeTAD	0.0	16.31	0.91	0.45	6.71	0.01
	0.1	24.51	1.01	0.47	11.75	0.00
	0.5	14.96	1.01	0.59	9.07	0.01
	1.0	16.73	0.97	0.48	7.85	0.02
	5.0	16.31	0.91	0.45	6.71	0.02
P3HT	0.0	16.73	0.95	0.45	7.14	0.15
	0.1	15.97	0.85	0.59	8.01	0.02
	0.3	16.85	0.85	0.58	8.30	0.00
	0.5	19.44	0.86	0.58	9.70	0.13
	0.7	16.28	0.84	0.46	6.15	0.15
	1.0	14.47	0.86	0.48	5.97	0.20

We then measured devices with F4-TCNQ:P3HT as HTM layer. The F4-TCNQ lowest unoccupied molecular orbital (LUMO) is deeper than the P3HT highest occupied molecular orbital

(HOMO), inducing efficient electron transfer and an ionised complex ($P3HT^{+}$) that increases the electrical conductivity [36,45]. The doping effect confirmed in Spiro-OMeTAD has also been observed in the P3HT (best devices in **Table 1** and **Figure 2**). The average PCE on 4 devices are 7.00 ± 0.19, 7.90 ± 0.13, 8.21 ± 0.10, 9.53 ± 0.24, 5.80 ± 0.40, 5.55 ± 0.48 for undoped, 0 wt%, 0.1 wt%, 0.3 wt%, 0.5 wt%, 0.7 wt%, and 1 wt% F4-TCNQ doping respectively. The current increases with the dopant concentration up to 0.5 wt% then it decreases. In the case of 0.1 and 0.3 wt% doping, an excellent balance between current and voltage is achieved, clearly expressed by the improvement of the Fill Factor (FF). Raising the molecular doping, a worsening in the overall performances occurs: the hysteresis in the IV measurements reappears for doping at 0.5 wt%, reaching 0.20 for the 1wt% doping. For the intermediate doping, 0.3 wt%, the charge extraction is so effective that the hysteresis in the measures, enhanced by the decrease of charge recombination, is squeezed [50-52]. We can assume that, once a certain percentage of doping has been reached, aggregates will start to be created at the interface, affecting the hysteresis. Further increasing the doping, it is evident that the worsening of the performance is due to the short-circuit current lowering and FF reduction (**Figure 2**).

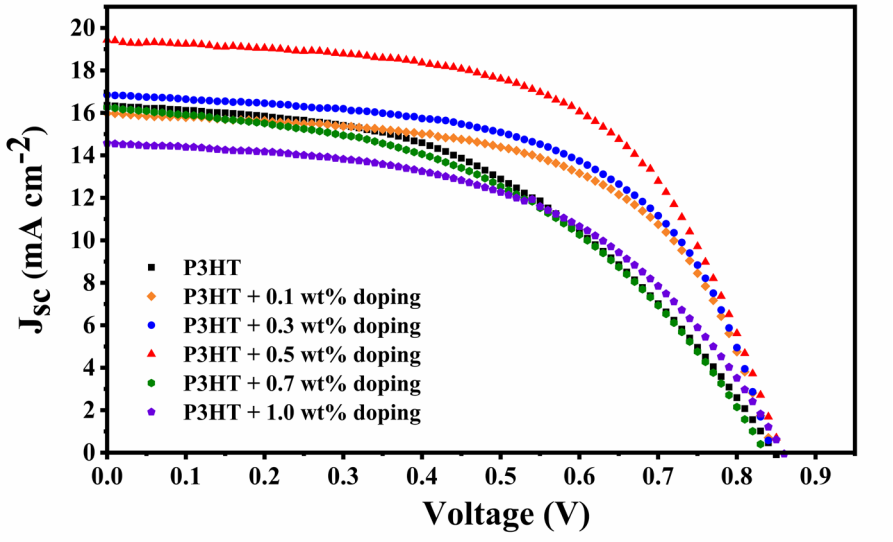

Figure 2. Characteristic curves of the best performing devices.

The fill-factor is affected by the shunt (R_{sh}) and the series resistance (R_s), by the recombination current and the reverse saturation current [44]. Here we give a simple evaluation of R_{sh} and R_s, considering the slopes of the characteristic curves where the voltage and current are null, respectively. Even from this trivial evaluation (**Figure 3**), relevant information can be obtained: (i) R_{sh} remains comparable along the series, except for the worst-performing devices, 1wt% doping, in which the shunt resistance decreases indicating the arising of a leakage path for current flow [44]; (ii) R_s and HI follow the same trend, supporting the assumption that the optimal doping level is obtained when the increase in the charge extraction is still able to balance the detrimental effect of aggregate formation at the interface between the charge extraction and the active layers.

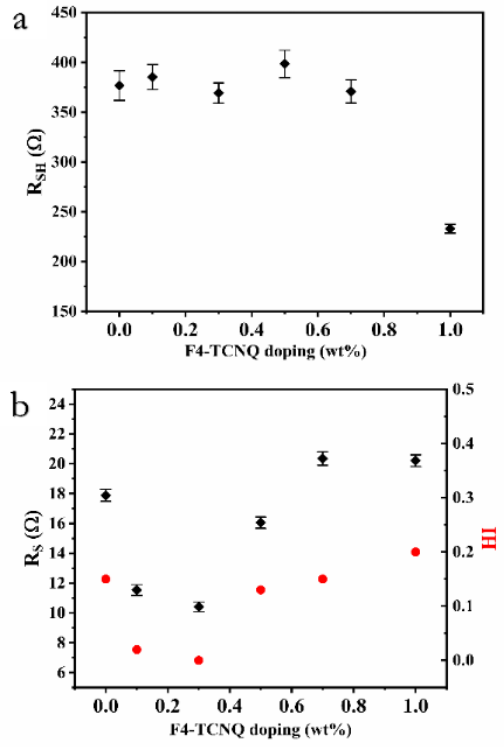

Figure 3. a) Shunt (R_{sh}) and b) Series resistance (R_s) evaluated assuming the single diode model.

External Quantum Efficiency confirms the photovoltaic performances (**Figure 4**): the integrated current J_{sc} was found 15.45, 16.57, 19.18 mA cm^{-2} for undoped P3HT, 0.3wt%-doped P3HT and 0.5wt%-doped P3HT respectively, ensuring the reliability of the photovoltaic characterisation. The more significant gain that comes from the doping is visible for wavelengths greater than 600 nm: this can be compatible with the assumption that the P3HT Fermi level is shifting close its HOMO level [53,54].

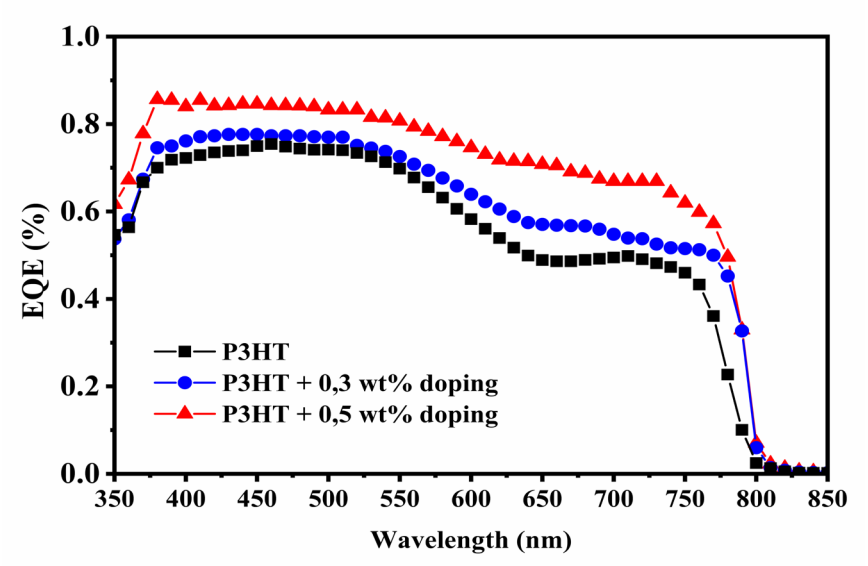

Figure 4. External Quantum Efficiency (EQE) spectra of the best performing devices.

The characteristic curves acquisitions in time, in nitrogen and air, for pristine and 0.3wt%-doped P3HT-based devices are shown in **Figure 5**. The drastic performance improvement is related to the P3HT interaction with oxygen, quickly forming a charge transfer complex, that increases the hole

concentration [55,56]. The addition of F4-TCNQ led to a further slip of P3HT Fermi level near its HOMO level [53,54], increasing the depletion layer built-in voltage and, therefore, improving the device performances [55]. The doping effect is apparent also when a 0.3wt%-doped P3HT is not exposed to air (**Figure 5**). The performance is remarkably higher than the pristine one, and the oxygen doping effect on P3HT is mitigated. These results confirm that p-type doping of P3HT with F4-TCNQ act as efficient HTM layers in solar cells perovskites. We suggest that the P3HT stability in air has been improved by the P3HT bonding with F4-TCNQ, that starts in the precursor solution, and evolves in a semi-crystalline phase which may be less inclined to react with oxygen.

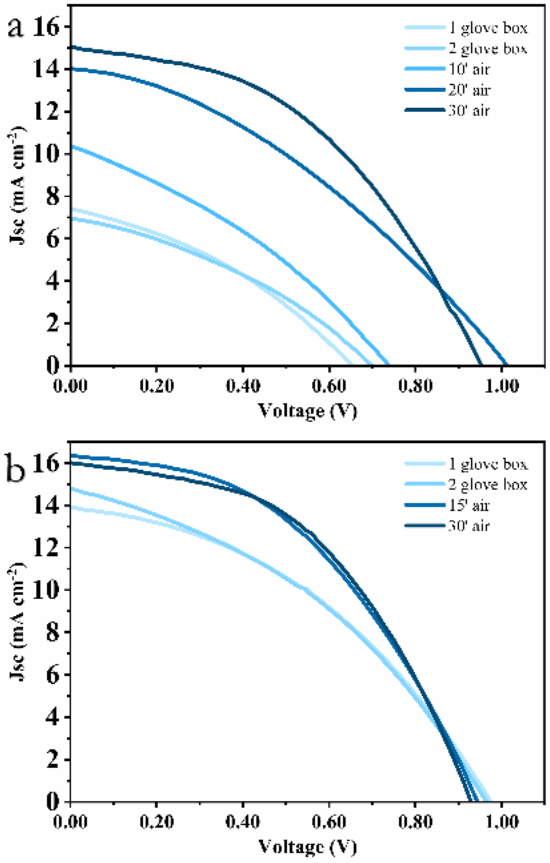

Figure 5. Characteristic curves acquisitions in time for a) pristine- and b) 0.3wt%-doped P3HT-based devices.

In **Figure 6,** the average PCE in time for 4 devices employing 0.3 wt% F4-TCNQ:P3HT, stored in dark in a nitrogen glove box and measured after 30 minutes in air, are reported. On average they retain 99% PCE after 1 week and 97% after 1 month of the first performance, showing remarkable durability.

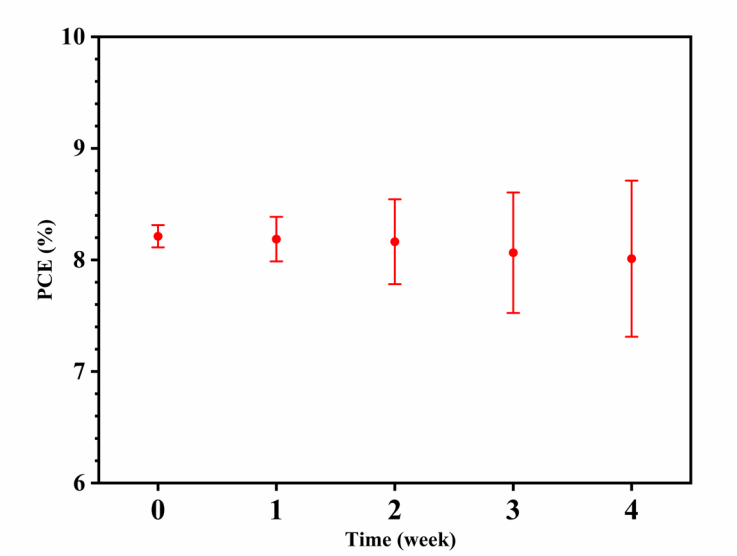

Figure 6. Average PCE in time for 4 devices employing 0.3 wt% F4-TCNQ:P3HT, stored in dark in a Nitrogen glove box, and measured after 30 minutes in air.

In order to investigate the nature of this increase in performance, we investigated the optical and the morphology properties of the molecular doped HTM thin film. The UV-Vis absorption spectra (**Figure 7**) does not show the polaronic bands characteristic of the heavily doped P3HT, consistent with the weak doping regime of F4-TCNQ:P3HT films [57]. Note that P3HT-F4TCNQ do form charged complex even in the weak doping regime [57], which explain the slight improvement in electrical conductivity of F4-TCNQ:P3HT-based devices.

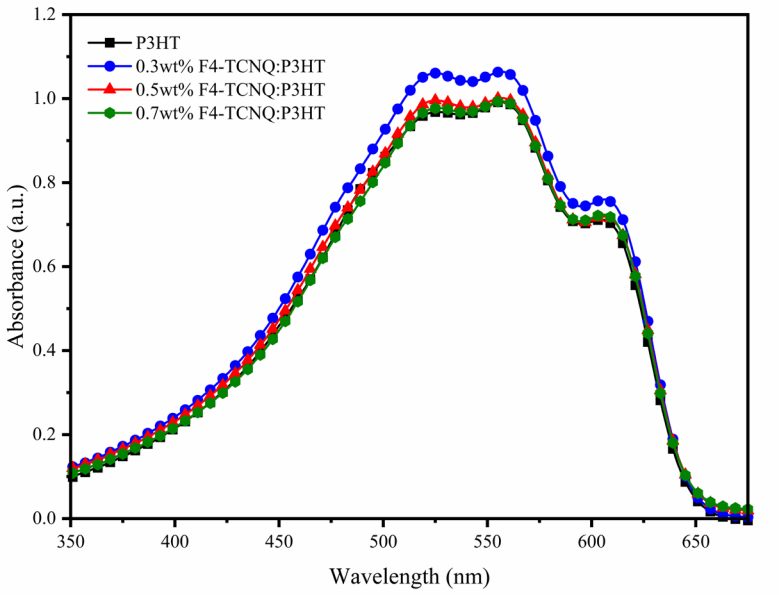

Figure 7. UV-Vis absorption spectra of F4-TCNQ:P3HT thin film.

Peer-reviewed version available at Metals 2019, 10, 14; doi:10.3390/met10010014

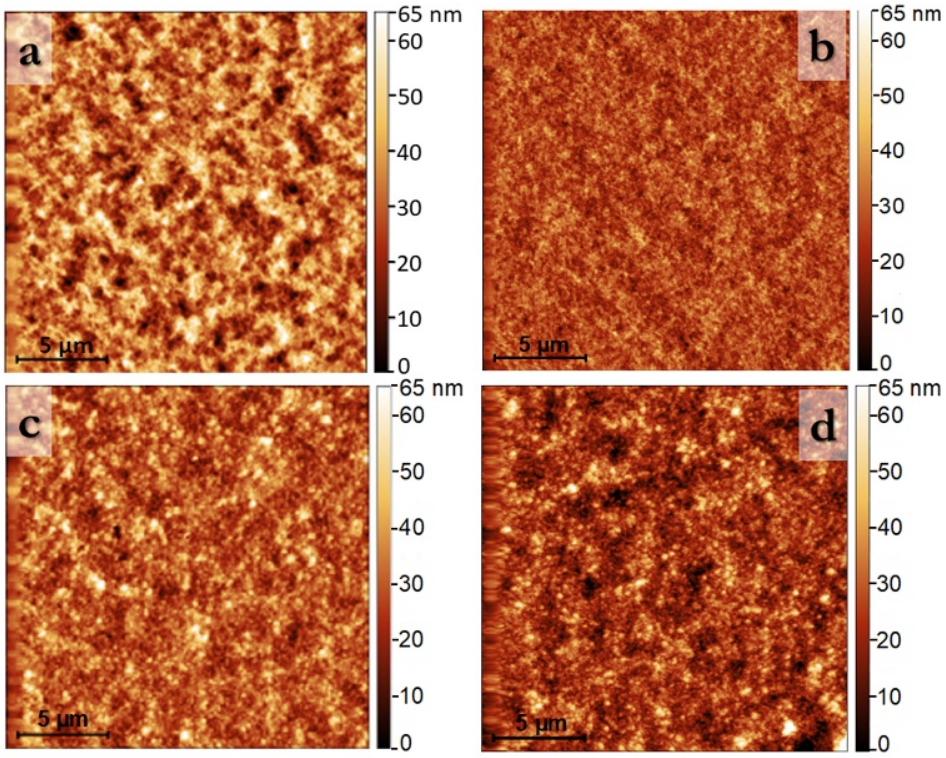

Figure 8. AFM images of a) pristine P3HT, b) 0.3 wt%, c) 0.5wt% and d) 0.7wt% F4-TCNQ:P3HT thin film.

The surface roughness, R_q, calculated by analysing the AFM images in **Figure 8**, is 11 nm, 6 nm, 8 nm, and 9 nm for pristine P3HT and 0.3wt%, 0.5 wt%, and 0.7 wt% F4-TCNQ:P3HT respectively. This slight increase in the film roughness is consistent with previous work on F4-TCNQ:P3HT films in the weak doping regime [57,58]. High dopant concentrations, can compromise the P3HT crystalline structure, making it amorphous, and so increasing the scattering centres and the density of traps [53]. Gao et al. [59], reported that formation of J-aggregate makes the polymer backbone more rigid: they suggested that F4-TCNQ adds holes to the polymer, shifting the equilibrium in favour of aggregated state formation. Considering this and studying the doping aggregation, Jacobs et al. [58], concluded that the segregation of dopant, and the resulting pathways for the charge conduction are exactly the responsible for the higher conductivities, but only at low doping levels. In high doping condition, F4-TCNQ forms isolated domains; therefore, most of the charge carriers remain too strongly bound to be available for the electrical conduction [60]. The reported F4-TCNQ:P3HT-based devices with a dopant concentration higher than 0.5 wt% show a decrease in performance due to the generation of aggregates, acting like traps for the charge carriers, affecting hysteresis and performance. In 0.3 wt% molecular doped P3HT, the loss in charge carriers caused by the aggregate formation is still well balanced by the charge extraction increase, leading to devices with high performances and without hysteresis.

5. Conclusions

F4-TCNQ has been employed as an additive in a small molecule and polymer HTM. We tested F4-TCNQ doping, in various concentration, in the c-TiO_2:PHJ configuration. We employed a pinhole-free $CH_3NH_3PbI_3$ layer with reduced surface defects and large grain size, that can generate high photovoltaic performance independently on the direction of voltage scan. We have confirmed that the molecular doping of the HTM is highly effective both using Spiro-OMeTAD and P3HT, but above all that F4-TCNQ employment in P3HT-based devices increases and stabilises the performances. F4-TCNQ doping generates the ionised complex $P3HT^+$ that increases the P3HT conductivity and decreases the charge recombination. We have demonstrated that molecular doping mechanism is

more reliable than oxidation doping, as it happens in Li-TFSI doped Spiro-OMeTAD and pristine P3HT. We showed that the F4-TCNQ doping could also mitigate the oxygen effect on P3HT. We attribute the increase in conductivities to the segregation of dopant, but only at low doping levels in order to avoid the aggregates' formation at the interface between the perovskite and the HTM, firstly affecting the hysteresis, then the overall performances. We verify that the F4-TCNQ employment in P3HT devices stabilises the performances, making the solar cell capable of delivering high performance over a long time. We are confident that a fine optimisation and engineering of F4-TCNQ doping in P3HT based perovskite solar cells would lead to highly efficient devices, with long-term stability.

Author Contributions: conceptualization, V.T., T.D., A.R. and S.C.; methodology, V.T. and S.C.; validation, V.T., A.R. and S.C.; formal analysis, V.T. and T.D.; investigation, V.T. and N.M.; data curation, V.T. and N.M.; writing—original draft preparation, V.T. and T.D.; writing—review and editing, V.T., T.D., O.F.; visualization, V.T.; supervision, O.F., A.R. and S.C.; project administration, A.R. and V.T.; funding acquisition, V.T., O.F., A.R and S.C..

Funding: V.T. acknowledges the European union's Horizon 2020 research and innovation program under the Marie Skłodowska-Curie grant agreement N° 798271. S.C. acknowledges Regione Puglia and ARTI for funding FIR – future in research project "PeroFlex" project no. LSBC6N4. A.R. gratefully acknowledges SIR project "Two-Dimensional Colloidal Metal Dichalcogenides based Energy-Conversion Photovoltaics" (2D ECO), Bando SIR (Scientific Independence of young Researchers) 2014 MIUR Decreto Direttoriale 23 Gennaio 2014 no. 197 (project number RBSI14FYVD, CUP: B82I15000950008) for funding. O.F. acknowledges the Royal Society for his University Research Fellowship (UF140372)

Acknowledgements: The authors acknowledge Sonia Carallo for technical support.

Conflicts of Interest: The authors declare no conflict of interest. The funders had no role in the design of the study; in the collection, analyses, or interpretation of data; in the writing of the manuscript, or in the decision to publish the results.

References

1. Colella, S.; Mazzeo, M.; Rizzo, A.; Gigli, G.; Listorti, A. The bright side of perovskites. *The Journal of Physical Chemistry Letters* **2016**, *7*, 4322-4334.
2. Sutherland, B.R.; Sargent, E.H. Perovskite photonic sources. *Nature Photonics* **2016**, *10*, 295.
3. Zhang, W.; Eperon, G.E.; Snaith, H.J. Metal halide perovskites for energy applications. *Nature Energy* **2016**, *1*, 16048.
4. Snaith, H.J. Present status and future prospects of perovskite photovoltaics. *Nature Materials* **2018**, *17*, 372-376.
5. Ansari, M.I.H.; Qurashi, A.; Nazeeruddin, M.K. Frontiers, opportunities, and challenges in perovskite solar cells: a critical review. *Journal of Photochemistry and Photobiology C: Photochemistry Reviews* **2018**, *35*, 1-24.
6. NREL. The national renewable energy laboratory. Best research-cell efficiency chart. https://www.nrel.gov/pv/cell-efficiency.html
7. Rehman, W.; McMeekin, D.P.; Patel, J.B.; Milot, R.L.; Johnston, M.B.; Snaith, H.J.; Herz, L.M. Photovoltaic mixed-cation lead mixed-halide perovskites: Links between crystallinity, photo-stability and electronic properties. *Energy & Environmental Science* **2017**, *10*, 361-369.
8. Wang, Z.; McMeekin, D.P.; Sakai, N.; van Reenen, S.; Wojciechowski, K.; Patel, J.B.; Johnston, M.B.; Snaith, H.J. Efficient and air-stable mixed-cation lead mixed-halide perovskite solar cells with n-doped organic electron extraction layers. *Advanced Materials* **2017**, *29*, 1604186.
9. Rong, Y.; Hu, Y.; Mei, A.; Tan, H.; Saidaminov, M.I.; Seok, S.I.; McGehee, M.D.; Sargent, E.H.; Han, H. Challenges for commercializing perovskite solar cells. *Science* **2018**, *361*, eaat8235.
10. Salhi, B.; Wudil, Y.S.; Hossain, M.K.; Al-Ahmed, A.; Al-Sulaiman, F.A. Review of recent developments and persistent challenges in stability of perovskite solar cells. *Renewable and Sustainable Energy Reviews* **2018**, *90*, 210-222.

11. Sani, F.; Shafie, S.; Lim, H.N.; Musa, A.O. Advancement on lead-free organic-inorganic halide perovskite solar cells: A review. *Materials* **2018**, *11*, 1008.
12. Nguyen, W.H.; Bailie, C.D.; Unger, E.L.; McGehee, M.D. Enhancing the hole-conductivity of spiro-ometad without oxygen or lithium salts by using Spiro(TFSI)$_2$ in perovskite and dye-sensitized solar cells. *Journal of the American Chemical Society* **2014**, *136*, 10996-11001.
13. Li, Z.; Xiao, C.; Yang, Y.; Harvey, S.P.; Kim, D.H.; Christians, J.A.; Yang, M.; Schulz, P.; Nanayakkara, S.U.; Jiang, C.-S., *et al.* Extrinsic ion migration in perovskite solar cells. *Energy & Environmental Science* **2017**, *10*, 1234-1242.
14. Jung, E.H.; Jeon, N.J.; Park, E.Y.; Moon, C.S.; Shin, T.J.; Yang, T.-Y.; Noh, J.H.; Seo, J. Efficient, stable and scalable perovskite solar cells using poly(3-hexylthiophene). *Nature* **2019**, *567*, 511-515.
15. Bi, D.; Yang, L.; Boschloo, G.; Hagfeldt, A.; Johansson, E.M.J. Effect of different hole transport materials on recombination in $CH_3NH_3PbI_3$ perovskite-sensitized mesoscopic solar cells. *The Journal of Physical Chemistry Letters* **2013**, *4*, 1532-1536.
16. Domanski, K.; Correa-Baena, J.-P.; Mine, N.; Nazeeruddin, M.K.; Abate, A.; Saliba, M.; Tress, W.; Hagfeldt, A.; Grätzel, M. Not all that glitters is gold: metal-migration-induced degradation in perovskite solar cells. *ACS Nano* **2016**, *10*, 6306-6314.
17. Di Giacomo, F.; Razza, S.; Matteocci, F.; D'Epifanio, A.; Licoccia, S.; Brown, T.M.; Di Carlo, A. High efficiency $CH_3NH_3PbI_{(3-x)}Cl_x$ perovskite solar cells with poly(3-hexylthiophene) hole transport layer. *Journal of Power Sources* **2014**, *251*, 152-156.
18. Zhu, Z.; Bai, Y.; Zhang, T.; Liu, Z.; Long, X.; Wei, Z.; Wang, Z.; Zhang, L.; Wang, J.; Yan, F., *et al.* High-performance hole-extraction layer of sol–gel-processed nio nanocrystals for inverted planar perovskite solar cells. *Angewandte Chemie International Edition* **2014**, *53*, 12571-12575.
19. Søndergaard, R.; Hösel, M.; Angmo, D.; Larsen-Olsen, T.T.; Krebs, F.C. Roll-to-roll fabrication of polymer solar cells. *Materials Today* **2012**, *15*, 36-49.
20. Ratcliff, E.L.; Jenkins, J.L.; Nebesny, K.; Armstrong, N.R. Electrodeposited, "textured" poly(3-hexyl-thiophene) (e-P3HT) films for photovoltaic applications. *Chemistry of Materials* **2008**, *20*, 5796-5806.
21. Abbas, H.A.; Kottokkaran, R.; Ganapathy, B.; Samiee, M.; Zhang, L.; Kitahara, A.; Noack, M.; Dalal, V.L. High efficiency sequentially vapor grown n-i-p $CH_3NH_3PbI_3$ perovskite solar cells with undoped P3HT as p-type heterojunction layer. *APL Mater.* **2015**, *3*, 016105.
22. Genco, A.; Mariano, F.; Carallo, S.; Guerra, V.L.P.; Gambino, S.; Simeone, D.; Listorti, A.; Colella, S.; Gigli, G.; Mazzeo, M. Fully vapor-deposited heterostructured light-emitting diode based on organo-metal halide perovskite. *Advanced Electronic Materials* **2016**, *2*, n/a-n/a.
23. Jacobs, I.E.; Moulé, A.J. Controlling molecular doping in organic semiconductors. *Advanced Materials* **2017**, *29*, 1703063.
24. Larrain, F.A.; Fuentes-Hernandez, C.; Chou, W.-F.; Rodriguez-Toro, V.A.; Huang, T.-Y.; Toney, M.F.; Kippelen, B. Stable solvent for solution-based electrical doping of semiconducting polymer films and its application to organic solar cells. *Energy & Environmental Science* **2018**, *11*, 2216-2224.
25. Gatti, T.; Casaluci, S.; Prato, M.; Salerno, M.; Di Stasio, F.; Ansaldo, A.; Menna, E.; Di Carlo, A.; Bonaccorso, F. Boosting perovskite solar cells performance and stability through doping a poly-3(hexylthiophene) hole transporting material with organic functionalized carbon nanostructures. *Advanced Functional Materials* **2016**, *26*, 7443-7453.
26. Loiudice, A.; Rizzo, A.; Biasiucci, M.; Gigli, G. Bulk heterojunction versus diffused bilayer: The role of device geometry in solution p-doped polymer-based solar cells. *The Journal of Physical Chemistry Letters* **2012**, *3*, 1908-1915.
27. Gheno, A.; Vedraine, S.; Ratier, B.; Bouclé, J. Π-conjugated materials as the hole-transporting layer in perovskite solar cells. *Metals* **2016**, *6*, 21.
28. Luo, J.; Jia, C.; Wan, Z.; Han, F.; Zhao, B.; Wang, R. The novel dopant for hole-transporting material opens a new processing route to efficiently reduce hysteresis and improve stability of planar perovskite solar cells. *Journal of Power Sources* **2017**, *342*, 886-895.
29. Liu, D.; Li, Y.; Yuan, J.; Hong, Q.; Shi, G.; Yuan, D.; Wei, J.; Huang, C.; Tang, J.; Fung, M.-K. Improved performance of inverted planar perovskite solar cells with F4TCNQ doped PEDOT:PSS hole transport layers. *Journal of Materials Chemistry A* **2017**, *5*, 5701-5708.
30. Pfeiffer, M.; Beyer, A.; Fritz, T.; Leo, K. Controlled doping of phthalocyanine layers by cosublimation with acceptor molecules: a systematic seebeck and conductivity study. *Applied Physics Letters* **1998**, *73*, 3202-3204.

31. Colsmann, A.; Junge, J.; Kayser, C.; Lemmer, U. Organic tandem solar cells comprising polymer and small-molecule subcells. *Applied Physics Letters* **2006**, *89*, 203506.
32. Aziz, E.F.; Vollmer, A.; Eisebitt, S.; Eberhardt, W.; Pingel, P.; Neher, D.; Koch, N. Localized charge transfer in a molecularly doped conducting polymer. *Advanced Materials* **2007**, *19*, 3257-3260.
33. Yim, K.-H.; Whiting, G.L.; Murphy, C.E.; Halls, J.J.M.; Burroughes, J.H.; Friend, R.H.; Kim, J.-S. Controlling electrical properties of conjugated polymers via a solution-based p-type doping. *Advanced Materials* **2008**, *20*, 3319-3324.
34. Lee, J.H.; Yoon, S.; Ko, M.S.; Lee, N.; Hwang, I.; Lee, M.J. Improved performance of organic photovoltaic devices by doping F4TCNQ onto solution-processed graphene as a hole transport layer. *Organic Electronics* **2016**, *30*, 302-311.
35. Hwang, S.; Potscavage Jr, W.J.; Nakamichi, R.; Adachi, C. Processing and doping of thick polymer active layers for flexible organic thermoelectric modules. *Organic Electronics* **2016**, *31*, 31-40.
36. Zhang, Y.; Elawad, M.; Yu, Z.; Jiang, X.; Lai, J.; Sun, L. Enhanced performance of perovskite solar cells with P3HT hole-transporting materials via molecular p-type doping. *RSC Advances* **2016**, *6*, 108888-108895.
37. Hawash, Z.; Ono, L.K.; Qi, Y. Recent advances in spiro-meotad hole transport material and its applications in organic–inorganic halide perovskite solar cells. *Advanced Materials Interfaces* **2018**, *5*, 1700623.
38. Huang, L.; Hu, Z.; Xu, J.; Zhang, K.; Zhang, J.; Zhang, J.; Zhu, Y. Efficient and stable planar perovskite solar cells with a non-hygroscopic small molecule oxidant doped hole transport layer. *Electrochimica Acta* **2016**, *196*, 328-336.
39. Liu, M.; Johnston, M.B.; Snaith, H.J. Efficient planar heterojunction perovskite solar cells by vapour deposition. *Nature* **2013**, *501*, 395-398.
40. Trifiletti, V.; Manfredi, N.; Listorti, A.; Altamura, D.; Giannini, C.; Colella, S.; Gigli, G.; Rizzo, A. Engineering TiO_2/perovskite planar heterojunction for hysteresis-less solar cells. *Advanced Materials Interfaces* **2016**, *3*, 1600493.
41. Trifiletti, V.; Cannavale, A.; Listorti, A.; Rizzo, A.; Colella, S. Sequential deposition of hybrid halide perovskite starting both from lead iodide and lead chloride on the most widely employed substrates. *Thin Solid Films* **2018**, *657*, 110-117.
42. Guerra, V.L.P.; Altamura, D.; Trifiletti, V.; Colella, S.; Listorti, A.; Giannuzzi, R.; Pellegrino, G.; Condorelli, G.G.; Giannini, C.; Gigli, G., *et al.* Implications of TiO_2 surface functionalization on polycrystalline mixed halide perovskite films and photovoltaic devices. *J. Mater. Chem. A* **2015**, *3*, 20811-20818.
43. Motaung, D.E.; Malgas, G.F.; Arendse, C.J.; Mavundla, S.E.; Oliphant, C.J.; Knoesen, D. The influence of thermal annealing on the morphology and structural properties of a conjugated polymer in blends with an organic acceptor material. *Journal of Materials Science* **2009**, *44*, 3192-3197.
44. The physics of the solar cell. In Handbook of photovoltaic science and engineering, pp 82-129.
45. Duong, D.T.; Phan, H.; Hanifi, D.; Jo, P.S.; Nguyen, T.-Q.; Salleo, A. Direct observation of doping sites in temperature-controlled, p-doped P3HT thin films by conducting atomic force microscopy. *Advanced Materials* **2014**, *26*, 6069-6073.
46. Han, X.; Wu, Z.; Sun, B. Enhanced performance of inverted organic solar cell by a solution-based fluorinated acceptor doped P3HT:PCBM layer. *Organic Electronics* **2013**, *14*, 1116-1121.
47. Pingel, P.; Zhu, L.; Park, K.S.; Vogel, J.-O.; Janietz, S.; Kim, E.-G.; Rabe, J.P.; Brédas, J.-L.; Koch, N. Charge-transfer localization in molecularly doped thiophene-based donor polymers. *The Journal of Physical Chemistry Letters* **2010**, *1*, 2037-2041.
48. Deschler, F.; Riedel, D.; Deák, A.; Ecker, B.; von Hauff, E.; Da Como, E. Imaging of morphological changes and phase segregation in doped polymeric semiconductors. *Synthetic Metals* **2015**, *199*, 381-387.
49. Calado, P.; Telford, A.M.; Bryant, D.; Li, X.; Nelson, J.; O'Regan, B.C.; Barnes, P.R.F. Evidence for ion migration in hybrid perovskite solar cells with minimal hysteresis. *Nature Communications* **2016**, *7*, 13831.
50. Zhang, Y.; Liu, M.; Eperon, G.E.; Leijtens, T.C.; McMeekin, D.; Saliba, M.; Zhang, W.; de Bastiani, M.; Petrozza, A.; Herz, L.M., *et al.* Charge selective contacts, mobile ions and anomalous hysteresis in organic-inorganic perovskite solar cells. *Materials Horizons* **2015**, *2*, 315-322.
51. Kim, B.J.; Kim, M.-c.; Lee, D.G.; Lee, G.; Bang, G.J.; Jeon, J.B.; Choi, M.; Jung, H.S. Interface design of hybrid electron extraction layer for relieving hysteresis and retarding charge recombination in perovskite solar cells. *Advanced Materials Interfaces* **2018**, *5*, 1800993.

52. Ravishankar, S.; Gharibzadeh, S.; Roldán-Carmona, C.; Grancini, G.; Lee, Y.; Ralaiarisoa, M.; Asiri, A.M.; Koch, N.; Bisquert, J.; Nazeeruddin, M.K. Influence of charge transport layers on open-circuit voltage and hysteresis in perovskite solar cells. *Joule* **2018**, *2*, 788-798.
53. Salzmann, I.; Heimel, G.; Oehzelt, M.; Winkler, S.; Koch, N. Molecular electrical doping of organic semiconductors: fundamental mechanisms and emerging dopant design rules. *Accounts of Chemical Research* **2016**, *49*, 370-378.
54. Méndez, H.; Heimel, G.; Winkler, S.; Frisch, J.; Opitz, A.; Sauer, K.; Wegner, B.; Oehzelt, M.; Röthel, C.; Duhm, S., *et al.* Charge-transfer crystallites as molecular electrical dopants. *Nature Communications* **2015**, *6*, 8560.
55. Lei, X.; Zhang, F.; Song, T.; Sun, B. P-type doping effect on the performance of organic-inorganic hybrid solar cells. *Applied Physics Letters* **2011**, *99*, 233305.
56. Hintz, H.; Peisert, H.; Egelhaaf, H.J.; Chassé, T. Reversible and irreversible light-induced p-doping of P3HT by oxygen studied by photoelectron spectroscopy (XPS/UPS). *The Journal of Physical Chemistry C* **2011**, *115*, 13373-13376.
57. Duong, D.T.; Wang, C.; Antono, E.; Toney, M.F.; Salleo, A. The chemical and structural origin of efficient p-type doping in P3HT. *Organic Electronics* **2013**, *14*, 1330-1336.
58. Jacobs, I.E.; Aasen, E.W.; Oliveira, J.L.; Fonseca, T.N.; Roehling, J.D.; Li, J.; Zhang, G.; Augustine, M.P.; Mascal, M.; Moulé, A.J. Comparison of solution-mixed and sequentially processed P3HT:PCBM films: effect of doping-induced aggregation on film morphology. *Journal of Materials Chemistry C* **2016**, *4*, 3454-3466.
59. Gao, J.; Roehling, J.D.; Li, Y.; Guo, H.; Moulé, A.J.; Grey, J.K. The effect of 2,3,5,6-tetrafluoro-7,7,8,8-tetracyanoquinodimethane charge transfer dopants on the conformation and aggregation of poly(3-hexylthiophene). *Journal of Materials Chemistry C* **2013**, *1*, 5638-5646.
60. Pingel, P.; Neher, D. Comprehensive picture of *p*-type doping of P3HT with the molecular acceptor F_4TCNQ. *Physical Review B* **2013**, *87*, 115209.